

AD-A272 328 **ATION PAGE**


OMB No. 0704-0188



per regulations including the time for reviewing instructions, examining existing data sources, gathering and maintaining the data needed, and for completing and reviewing the collection of information. Send comments regarding this burden estimate or any other aspect of this collection of information, including suggestions for reducing this burden, to Washington Headquarters Service, Paperwork Reduction Project (0704-0188), Arlington, VA 22202-4302, and to the Office of Management and Budget, Paperwork Reduction Project (0704-0188), Washington, DC 20503.

1. AGENCY USE ONLY (Leave blank)		2. REPORT DATE 3-5 MARCH 1993	3. REPORT TYPE AND DATES COVERED MEETING SPEECH	
4. TITLE AND SUBTITLE EXPERIMENT AND SIMULATION OF SUB-0.25-UM RESIST PROCESSES FOR 193-NM LITHOGRAPHY			5. FUNDING NUMBERS  C — F19628-90-C-0002 PE —	
6. AUTHOR(S)  R.R.KUNZ, M.A. HARTNEY, R.W.OTTEN, JR.				
7. PERFORMING ORGANIZATION NAME(S) AND ADDRESS(ES)  Lincoln Laboratory, MIT P.O. Box 73 Lexington, MA 02173-9108			8. PERFORMING ORGANIZATION REPORT NUMBER  MS-10168	
9. SPONSORING/MONITORING AGENCY NAME(S) AND ADDRESS(ES)  ADVANCED RESEARCH PROJECTS AGENCY 3701 N. FAIRFAX DRIVE ARLINGTON, VA 20305			10. SPONSORING/MONITORING AGENCY REPORT NUMBER  ESC-TR-93-283	
11. SUPPLEMENTARY NOTES REPRINTED FROM OPTICAL/LASER MICROLITHOGRAPHY SPIE VOL.1927				
12a. DISTRIBUTION/AVAILABILITY STATEMENT  Approved for public release; distribution is unlimited.			12b. DISTRIBUTION CODE	
13. ABSTRACT (Maximum 200 words)  A model was developed to simulate the behavior of near-surface-imaged resist processes, with the emphasis on modeling of resist processes for 193 nm. Silylation, bilayer, and additive resist processes can all be simulated using this model. For the silylation process, the model was found to be in excellent agreement with experimentally observed silylated resist profiles. This model was used in combination with existing programs that calculate aerial images and single-layer resist profiles to predict process margins for 193-nm (0.5 NA) lithography. The results of our simulations for 0.25- $\mu$ m features indicate a depth of focus comparable to the Rayleigh limit ( $\pm 0.4 \mu$ m) for a single-layer resist process and up to two times this value for near-surface-imaged resists. Focus latitudes greater than the Rayleigh limit are predicted for 0.18- $\mu$ m features when using near-surface-imaged resists in conjunction with annular illumination.				
14. SUBJECT TERMS  PHOTOLITHOGRAPHY; SIMULATIONS; SILYLATION; MODELING			15. NUMBER OF PAGES 14	
			16. PRICE CODE	
17. SECURITY CLASSIFICATION OF REPORT Unclassified	18. SECURITY CLASSIFICATION OF THIS PAGE Unclassified	19. SECURITY CLASSIFICATION OF ABSTRACT Unclassified	20. LIMITATION OF ABSTRACT	

**PROCEEDINGS REPRINT**

 SPIE-The International Society for Optical Engineering

2

Reprinted from

***Optical/Laser Microlithography***

3-5 March 1993  
San Jose, California

**S** DTIC  
ELECTE  
NOV 09 1993  
**A**

This document has been approved  
for public release and sale; its  
distribution is unlimited.

**93-27267**



**Volume 1927**

©1993 by the Society of Photo-Optical Instrumentation Engineers  
Box 10, Bellingham, Washington 98227 USA. Telephone 206/676-3290.

This reprint may be reproduced to satisfy needs  
of U. S. Government agencies.

**93 11 5 117**

# Experiment and simulation of sub-0.25- $\mu\text{m}$ resist processes for 193-nm lithography

Roderick R. Kunz, Mark A. Hartney, and Richard W. Otten, Jr.

Lincoln Laboratory, Massachusetts Institute of Technology  
Lexington, MA 02173-9108

and

Eytan Barouch and Uwe Hollerbach

Program in Applied and Computational Mathematics  
Princeton University, Princeton, NJ 08544-1000

## ABSTRACT

A model was developed to simulate the behavior of near-surface-imaged resist processes, with the emphasis on modeling of resist processes for 193 nm. Silylation, bilayer, and additive resist processes can all be simulated using this model. For the silylation process, the model was found to be in excellent agreement with experimentally observed silylated resist profiles. This model was used in combination with existing programs that calculate aerial images and single-layer resist profiles to predict process margins for 193-nm (0.5 NA) lithography. The results of our simulations for 0.25- $\mu\text{m}$  features indicate a depth of focus comparable to the Rayleigh limit ( $\pm 0.4 \mu\text{m}$ ) for a single-layer resist process and up to two times this value for near-surface-imaged resists. Focus latitudes greater than the Rayleigh limit are predicted for 0.18- $\mu\text{m}$  features when using near-surface-imaged resists in conjunction with annular illumination.

## 1. INTRODUCTION

The next generation of integrated circuit devices, such as the 256-Mb DRAM, will require minimum feature sizes of 0.25  $\mu\text{m}$  printed over large fields. At present, leading candidate technologies for 0.25- $\mu\text{m}$  lithography include deep ultraviolet (DUV) steppers operating at 248 nm, with or without modified illumination, pupil filtering, and phase-shifting masks, as well as deep-deep-UV steppers that operate at 193 nm.<sup>1</sup> Many different factors need to be considered when evaluating each of these technologies; one critical factor to consider is process margin. In this paper, we calculate the exposure and defocus latitudes for one of these 0.25- $\mu\text{m}$  technologies, namely, 193-nm lithography, and evaluate these latitudes at smaller dimensions as well. The predictions are based upon empirical models that have been developed to simulate the behavior of existing resist processes and have been experimentally verified with low-NA optics. The development and experimental verification of the resist modeling are presented first, followed by the calculation of the exposure and defocus latitudes.

## 2. EXPERIMENTAL

### 2.1. Exposure tools

The bulk of the experimental work was performed using a stepper equipped with a 0.22-NA catadioptric lens.<sup>2</sup> This system was capable of 0.30- $\mu\text{m}$  resolution using conventional illumination and 0.15  $\mu\text{m}$  when used with a modified illumination scheme. However, its performance was not diffraction limited. This fact limited our ability to accurately calculate the aerial images obtained from the stepper, and therefore posed difficulties in comparing experimental results with the predictions of our model. Some exposures were also performed recently on a near-diffraction-limited 0.5-NA system, which is a 193-nm prototype of the Micrascan 92.

## 2.2. Resists

Several different resist processes have been developed for 193 nm, and the simulations are based on their performance characteristics. For the single-layer resist, a positive-tone chemically amplified acrylate resist has recently been reported.<sup>3</sup> Bilayer<sup>4</sup> and silylation<sup>5</sup> processes have also been developed. The bilayer process is negative tone, can employ either wet<sup>6</sup> or dry<sup>7</sup> development, and consists of an ultrathin layer of silicon-backbone polymer on top of an organic planarizing layer. The silylation process is positive tone, in contrast to the commercially available DESIRE<sup>8</sup> silylation process: and unlike the DESIRE process, the 193-nm silylation process consists of diffusion of a silylating reagent into the resist between thin (40-100 nm) laser-crosslinked areas at the resist surface. The resulting silylation profile is then dictated more by the diffusion characteristics than by the exposure profile,<sup>5</sup> and therefore silylation under the exposed (crosslinked) region may be possible. Figure 1 illustrates the effects of lateral diffusion, which is most observable at silylation times several times longer than those used for standard processing. These unique characteristics of the silylation process at 193 nm necessitate development of a silylation model not only to calculate process margins, but also to develop a better overall understanding of the process. Our earlier models indicated that the silylation profiles did not necessarily reflect the aerial image<sup>9</sup> but that the degree of anisotropy of the diffusion, which could result from swelling-induced stress, may play a role.

All three of these resist systems have sensitivity less than 50 mJ/cm<sup>2</sup> and demonstrated resolution to at least 0.20  $\mu$ m. Figure 2 shows representative scanning electron micrographs for each of the resist systems. The single-layer resist is shown in Figure 2(a), the silylation resist in Figure 2(b), and the bilayer resist in Figure 2(c).

## 3. SIMULATIONS

### 3.1. Aerial images

The aerial images used in the calculations were generated by either PROLITH/2, Version 2.02 (Ref. 10) or AIM (Aerial Image Model).<sup>11</sup> Use of PROLITH/2 aerial images both with the PROLITH/2 resist algorithms and the MOSES (Modeling of Surface Exposed Systems) resist algorithms (see below) allowed calculation of process latitudes for each of the resist approaches while using identical aerial images. AIM was used for comparison of illumination modes (circular vs annular) in conjunction with MOSES. The AIM output was in three dimensions, from which a two-dimensional crosssection of equal lines and spaces was taken.

For both the PROLITH/2 and AIM aerial images, the NA was fixed at 0.50, the partial coherence used was 0.60, and diffraction-limited performance was assumed. The feature sizes used for the calculations were 0.25, 0.20, and 0.18  $\mu$ m, corresponding to  $k_1$  factors of 0.65, 0.52, and 0.47, respectively. For the aerial images from AIM using annular illumination, the annulus inner and outer radii were set at values corresponding to partial coherence factors of 0.40 and 0.60, respectively. Figure 3 shows modulation transfer function (MTF) curves for circular vs annular illumination as a function of defocus for both 0.25- and 0.18- $\mu$ m lines and spaces. It is apparent that the degradation of the MTF induced by defocusing is smaller when annular illumination is used as compared to circular illumination. It is shown below that this advantage of annular illumination translates under certain conditions into a large defocus latitude when specific resists are employed.

### 3.2. Resist Simulations

The single-layer resist was simulated using PROLITH/2 Version 2.02. Although PROLITH/2 Version 2.02 has no specific provisions for modeling of chemically amplified resist systems, we input the measured Dill parameters (A, B, and C) and development parameters (minimum and maximum dissolution rates, dissolution selectivity) to simulate a "generic" single-layer resist whose behavior is similar to our resist. Future simulations of this resist system will be performed using models specifically designed to

simulate chemically amplified resists. We assumed an antireflective layer 48.25 nm thick and with a complex refractive index of  $2.0 + 0.6i$ . This hypothetical layer reduced the simulated substrate reflectivity from 55 to 8%. The surface-imaged systems were simulated using MOSES, a program recently developed at Lincoln Laboratory, described below. MOSES, like PROLITH/2, is an empirical model but is capable of simulating silylation,<sup>5</sup> wet-developed bilayer,<sup>6</sup> dry-developed bilayer,<sup>7</sup> and at-the-surface additive resist processes.<sup>12</sup>

MOSES simulates the bilayer process by using an anisotropic dissolution (or dry-development) step for the imaging layer, followed by an anisotropic pattern transfer step. An experimentally determined relationship between the dissolution rate and the volumetric absorbed dose is used to simulate the resist dissolution as a function of distance along the resist, depth into the resist, and time. The oxygen plasma etch algorithm includes a rapid initial step where the surface portion (10-20 nm) of the organosilicon layer is consumed and converted into  $\text{SiO}_2$ , followed by a slower, steady-state erosion of the  $\text{SiO}_2$ .<sup>13</sup> The etch selectivities (imaging layer vs planarizing layer) and absolute planarizing layer etch rates have been measured for etching with a parallel-plate reactive ion etcher, a magnetron etcher, an electron cyclotron resonance etcher, and a helical resonator etcher.<sup>14</sup> The data used to describe any of these systems can be used as input into the pattern transfer model.

MOSES calculates the silylation profiles using an isotropic Case II diffusion model<sup>9</sup> described by

$$dL/dt = K R(D) P \exp(-E/kT) \quad (1)$$

where  $dL/dt$  is the silylation rate of any given volume element,  $K$  is a preexponential constant,  $P$  is the silylating agent pressure,  $E$  is the activation energy for diffusion (as dictated by polymer relaxation for Case II diffusion),  $k$  is Boltzmann's constant,  $T$  is the temperature,  $R(D)$  is the experimentally determined dose-dependent diffusion rate normalized relative to the diffusion rate in unexposed polymer (where  $R(0) = 1$ ), and  $D$  is the volumetric absorbed dose in units of  $\text{mJ}/\text{cm}^3$ . Of these variables, all are experimentally measurable except for  $K$ , which is determined from the slope of a plot of experimentally measured  $L$  vs  $t$  data.

The shape of the swollen surface that results from the volume expansion upon silylation is assumed to be controlled by surface tension. We make this assumption because the silylation temperature is well above the glass transition temperature of the silylated polymer,<sup>15</sup> a condition where the surface tension is sufficient to induce mechanical deformation in the swollen resist. Given a fractional expansion coefficient (typically 40-50%), we determine the increase in area (volume in three dimensions) that would be necessary to describe this swelling and then create a circular (or cylindrical for a line in three dimensions) surface profile that has the appropriate area. This approach has worked well for simple structures and has been confirmed experimentally, as detailed below (Figure 4).

Diffusion anomalies that may result from swelling-induced stress or crazing are neglected in this model. By so doing, departure of the predicted from experimentally observed resist profiles can be used to provide insight into the extent of effects caused by these diffusion anomalies. Following calculation of the silylation profile, the same oxygen plasma etching algorithm used for the bilayer is applied here.

Figure 4 shows MOSES output as compared to an experimentally obtained silylation profile. The comparison is made for an oversilylated feature to allow better experimental measurement of the silylation profile. The differences between the experimental and simulated profiles are attributed either to discrepancies between the theoretical and actual aerial images or to diffusion anomalies related to stress. In either case, the agreement is quite good, indicating that the silylation model used in MOSES provides a close approximation to actual resist performance under our experimental conditions.

## 4. RESULTS

### 4.1. Exposure-defocus latitude

Exposure-defocus (E-D) trees<sup>16</sup> for both the aerial image and our resist systems were obtained

from the simulation packages described above. In the example at Figure 5, E-D trees for 0.25- $\mu\text{m}$  equal lines and spaces are shown. The required doses are normalized with respect to the open frame sensitivity. As expected, the high-contrast ultrathin bilayer process replicates the aerial image E-D tree most faithfully. The silylation process exhibits quite different behavior. Even though its total process space is large, the effective process window is limited by a focus-dependent dose bias. This is due to increased diffusion inhibition in the nominally unexposed regions at larger defocus values. When very high contrast aerial images are used, such as at zero defocus, some overexposure is necessary to limit lateral diffusion. Such overexposure was not required when using our 0.22-NA optics, but the lack of diffraction-limited performance could explain the discrepancy, in which case the model is only limited by our ability to calculate the appropriate aerial image. In addition, parameters such as the thickness of the oxygen-plasma-consumed layer and residual stepper flare will also affect the shape of the E-D tree. In the end, the presence of linewidth biases and nonlinearity in the silylation process will depend upon the processing conditions used. Recall that the model intentionally ignores any diffusion anomalies that may result from swelling-induced stress; this assumption may also contribute to differences observed between experiment and simulation. A full evaluation of this resist using diffraction-limited optics is required to fully understand the effects (if any) caused by swelling-induced stress. Until such tests are performed, the results presented for silylation are to be considered as a worst-case scenario. A complete summary of these calculations is shown for both 0.25- and 0.20- $\mu\text{m}$  features in Table 1.

#### 4.2. Effects of illumination

Alternative illumination schemes for steppers have been developed in recent years as a means for enhancing focus latitudes.<sup>17,18</sup> We have calculated E-D trees for our resist systems using both circular and annular illumination. The E-D trees for both silylation and bilayer resists are plotted in Figures 6 and 7, respectively. These results are also tabulated in Table 2.

### 5. DISCUSSION

Several results become apparent from our calculations. First, focus latitudes for each of the resist processes at 0.25  $\mu\text{m}$  are wide enough for practical implementation in manufacturing. Using near-surface-imaged resists in conjunction with annular illumination provides focus latitudes that approach 2  $\mu\text{m}$ . For imaging in the 0.18- to 0.20- $\mu\text{m}$  regime, near-surface-imaged resists and/or modified illumination will be necessary for practical application. Second, process biases may exist for the silylation, the extent of which depends on the exact nature of the diffusion of the silylating reagent. The present simulations assume no stress-induced diffusion anomalies in silylation — a worst-case assumption resulting in isotropic diffusion. Even so, the silylation process matches or even exceeds (particularly at low  $k_1$  factor) single-layer resist processes.

The near-surface-imaged resists enable focus latitudes 1.5 to 2 times greater than those for single-layer resists. This result is in agreement with earlier simulations normalized for feature width, NA, and wavelength.<sup>16</sup> Excimer laser lithography using 193-nm radiation is thus shown to be capable of manufacturing 0.25- $\mu\text{m}$  devices and well suited to play a major role at 0.18  $\mu\text{m}$  as well.<sup>1,19</sup>

### 6. ACKNOWLEDGMENTS

We thank L. M. Eriksen and C. A. Bukowski for their expert technical assistance, M. Rothschild for many useful discussions, S. Stanton for assistance with the 0.5-NA prototype stepper, D. Johnson for supplying the poly(4-trimethylsiloxystyrene), and Prof. S. P. Sawan for providing the differential scanning calorimetry. The Lincoln Laboratory portion of this work was supported by the Defense Advanced Research Projects Agency. The Princeton University portion of the work was sponsored by the Air Force Office of Scientific Research and by the Defense Advanced Research Projects Agency.

## 7. REFERENCES

1. M. Endo, K. Hashimoto, K. Yamashita, A. Katsuyama, T. Matsuo, Y. Tani, M. Sasago, and N. Nomura, IEDM Digest, presented at 1992 IEDM Conference, p. IEDM 92-45, 1992.
2. D. C. Shaver, D. M. Craig, C. Marchi, M. A. Hartney, and F. Goodall, Proc. SPIE 1674, 766 (1992).
3. R. R. Kunz, R. D. Allen, W. D. Hinsberg, and G. M. Wallraff, Proc. SPIE 1925, (1993).
4. R. R. Kunz, P. A. Bianconi, M. W. Horn, R. R. Paladugu, D. C. Shaver, D. A. Smith, and C. A. Freed, Proc. SPIE 1466, 218 (1991).
5. M. A. Hartney, D. W. Johnson, and A. C. Spencer, Proc. SPIE 1466, 238 (1991).
6. R. R. Kunz, M. W. Horn, R. B. Goodman, P. A. Bianconi, D. A. Smith, and J. R. Eshelman, J. Vac. Sci. Technol. B 10, 2554 (1992).
7. R. R. Kunz, M. W. Horn, R. B. Goodman, P. A. Bianconi, D. A. Smith, J. R. Eshelman, G. M. Wallraff, R. D. Miller, and E. J. Ginsberg, Proc. SPIE 1672, 385 (1992).
8. F. Coopmans and B. Roland, Proc. SPIE 633, 126 (1986).
9. M. A. Hartney, J. Vac. Sci. Technol. B, in press.
10. C. A. Mack, Proc. SPIE 538, 207 (1985).
11. E. Barouch, B. Bradie, U. Hollerbach, S. A. Orszag, and M. Peckerar, Proc. SPIE 1465, 586 (1991).
12. R. R. Kunz, D. J. Ehrlich, J. Melngailis, and M. W. Horn, Proc. Mater. Res. Soc. Symp. 236, 105 (1991).
13. M. A. Hartney, J. N. Chiang, D. S. Soane, D. W. Hess, and R. D. Allen, Proc. SPIE 1086, 150 (1989).
14. M. W. Horn, M. A. Hartney, and R. R. Kunz, Proc. SPIE 1672, 448 (1992).
15. The  $T_g$  of poly(4-trimethylsiloxystyrene) was measured by differential scanning calorimetry to be 130 °C. Accounting for plasticization resulting from the presence of residual solvent and silylating agent during silylation, a  $T_g$  of roughly 40 to 80 °C was calculated for the silylated resin.
16. B. Lin, Proc. SPIE 1463, 42 (1991).
17. N. Shiraishi, S. Hirukawa, Y. Takeuchi, N. Magome, Proc. SPIE 1674, 741 (1992).
18. K. Tounai, H. Tanabe, H. Nozue, K. Kasema, Proc. SPIE 1674, 753 (1992).
19. M. Rothschild, R. B. Goodman, M. A. Hartney, M. W. Horn, R. R. Kunz, J. H. C. Sedlacek, and D. C. Shaver, J. Vac. Sci. Technol. B 10, 2989 (1992).

TABLE 1

Resist	Focus Latitude at 10% Exposure Latitude	Exposure Latitude at Zero Defocus	Maximum Focus Latitude
-----0.25- $\mu$ m Lines and Spaces-----			
Single layer	0.96 $\mu$ m	19%	1.28 $\mu$ m
Silylation	0.92 $\mu$ m	51%	1.12 $\mu$ m
Bilayer	1.52 $\mu$ m	48%	1.84 $\mu$ m
-----0.20- $\mu$ m Lines and Spaces-----			
Single Layer	0.16 $\mu$ m	5%	0.34 $\mu$ m
Silylation	0.86 $\mu$ m	35%	1.14 $\mu$ m
Bilayer	1.06 $\mu$ m	38%	1.66 $\mu$ m

Table 1. Process margins for single-layer, silylation, and bilayer resist processes. The process margins were defined as those conditions that are required to print the desired feature size to within 10% of its desired dimension. The calculations used for the silylation process had implicit assumptions regarding the silylating agent diffusion and should be considered as a worst-case scenario (see text). The focus latitudes listed here allow for defocusing in both directions and therefore are twice as large as those in Figure 5. The 10% exposure latitude refers to  $\pm 5\%$ .

Accession For	
NTIS CRA&I	<input checked="" type="checkbox"/>
DTIC TAB	<input type="checkbox"/>
Unannounced	<input type="checkbox"/>
Justification	
By	
Distribution /	
Availability Codes	
Dist	Avail and/or Special
A-1	20

DTIC QUALITY INSPECTED 8



TABLE 2

Resist		Focus Latitude at 10% Exposure Latitude	Exposure Latitude at Zero Defocus	Maximum Focus Latitude
-----0.25- $\mu$ m Lines and Spaces-----				
Silylation	Circular	1.00 $\mu$ m	51%	1.28 $\mu$ m
	Annular	1.34 $\mu$ m	37%	1.76 $\mu$ m
Bilayer	Circular	1.42 $\mu$ m	39%	1.84 $\mu$ m
	Annular	1.70 $\mu$ m	30%	2.20 $\mu$ m
-----0.18- $\mu$ m Lines and Spaces-----				
Silylation	Circular	0.84 $\mu$ m	27%	1.14 $\mu$ m
	Annular	0.80 $\mu$ m	23%	1.10 $\mu$ m
Bilayer	Circular	0.88 $\mu$ m	27%	1.52 $\mu$ m
	Annular	1.24 $\mu$ m	23%	2.02 $\mu$ m

Table 2. Comparison of circular and annular illumination schemes for both the silylation and bilayer resist processes. The slight decrease in performance for the silylation process is the result of feature-size biases that occur when the silylating agent diffusion is assumed to be totally isotropic (see text). The focus latitudes listed here allow for defocusing in both directions, and therefore are twice as large as those shown in Figures 6 and 7. The small differences between the values listed in Tables 1 and 2 for 0.25- $\mu$ m features obtained with circular illumination in silylation and bilayer resists are attributed to the differences between the aerial images calculated with PROLITH/2 (Table 1) and AIM (Table 2).

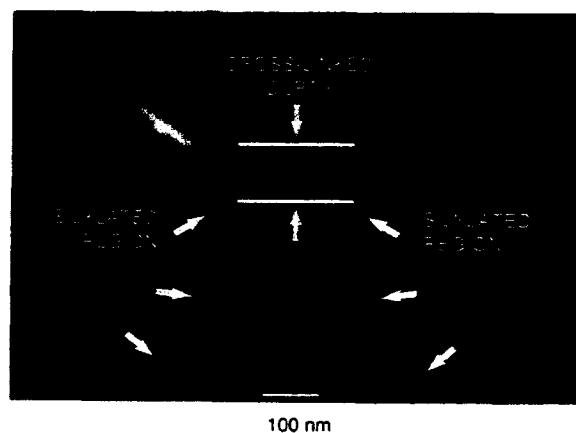


Figure 1. Cross-sectional scanning electron micrograph of an oversilylated nominally 1.0- $\mu\text{m}$  line-and-space structure imaged in poly(vinylphenol) at 193 nm. The silylation time was 5 min compared to a normal silylation time of 1 to 2 min. Note evidence of lateral diffusion by the silylating agent, which narrows the unsilylated width. The apparent silylation in the unsilylated area is a combination of gold (40 nm) deposited to prevent specimen charging in the electron microscope and a small amount of silylation (10-20 nm).

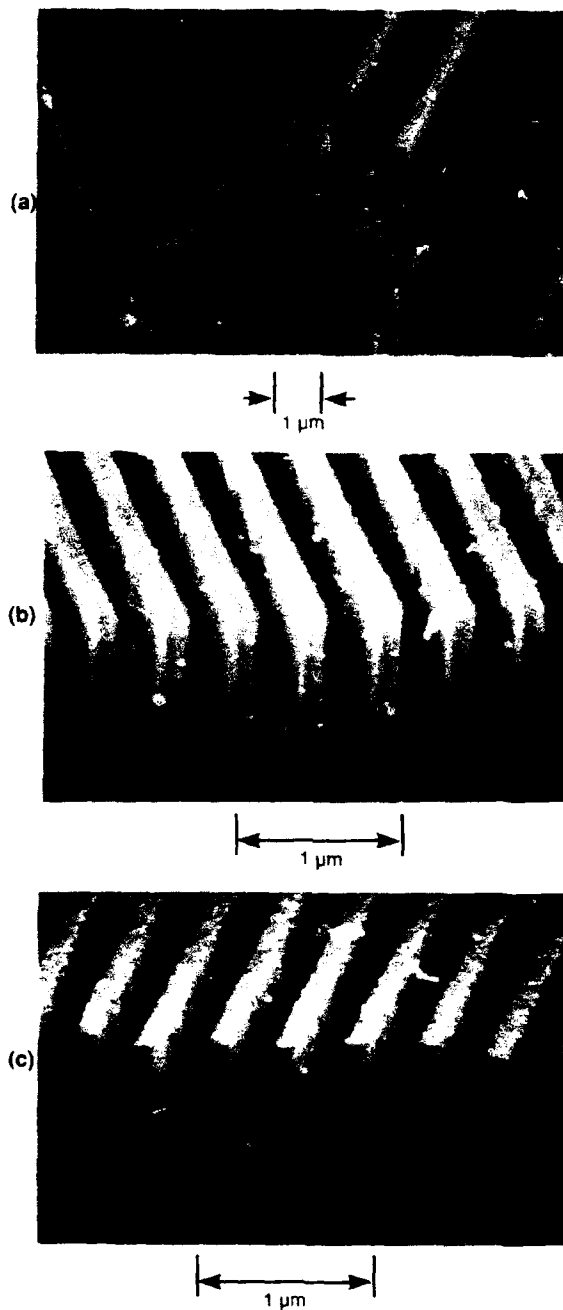


Figure 2. (a) 0.3- $\mu\text{m}$  features printed in 193-nm single-layer resist using a 0.50-NA stepper with conventional illumination. (b) 0.2- $\mu\text{m}$  line-and-space pattern in poly(vinylphenol) printed using the silylation process. The imaging was performed in a 0.22-NA system equipped with modified illumination which effectively doubled the spatial frequency. (c) 0.2- $\mu\text{m}$  line-and-space pattern using a bilayer resist and the same imaging system and method as in (b).

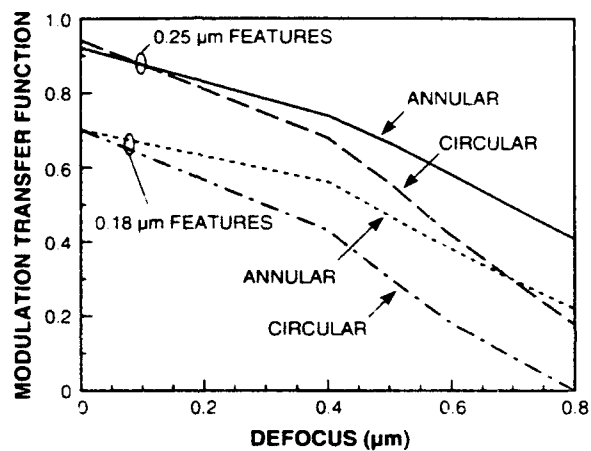
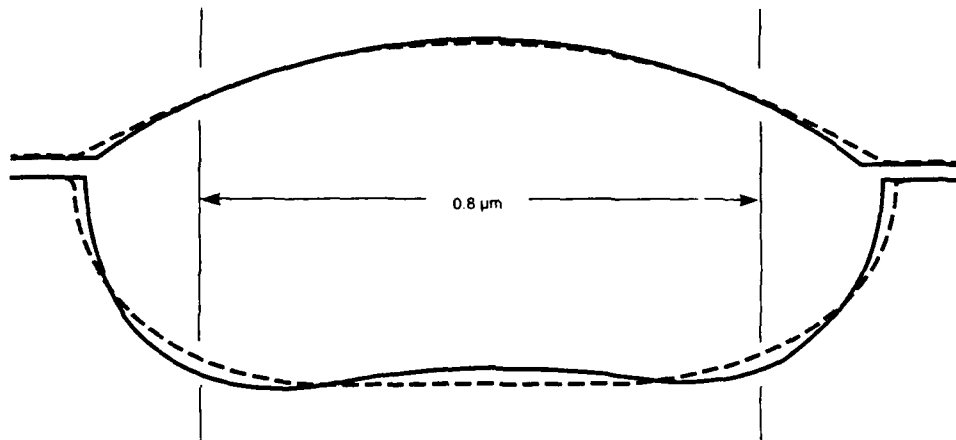



Figure 3. Modulation transfer function (MTF) as a function of defocus for a 0.5-NA, 193-nm stepper for both 0.25- and 0.18- $\mu\text{m}$  line-and-space patterns. For each feature size the MTF for both circular and annular illumination schemes is shown. For the circular illumination,  $\sigma = 0.6$ . For the annular illumination, the inner and outer radii of the annulus correspond to  $\sigma_i = 0.4$  and  $\sigma_o = 0.6$ .

MOSES SIMULATION OF SILYLATION  
OVER-SILYLATED 0.8- $\mu$ m GRATING LINE



		<u>RESIST</u>	<u>EXPOSURE*</u>	<u>SILYLATION</u>	<u>OPTICS</u>
	EXPERIMENT	PVP	350 PULSES	DMSDMA 105/2/10	0.22 NA, ABERRATED, OBSCURED
	CALCULATION	PVP	80 mJ/cm <sup>2</sup>	DMSDMA 105/2/10	0.22 NA, DIFF. LIMITED

\* USING OPEN-FRAME AERIAL IMAGES. MODELLED SENSITIVITY IS  
WITHIN 7% OF EXPERIMENTALLY OBSERVED SENSITIVITY  
FOR SIMILAR SILYLATION CONDITIONS

Figure 4. Comparison of the MOSES silylation model with an experimentally measured silylation profile. The resist was poly(vinylphenol), the simulated exposure dose was 80 mJ/cm<sup>2</sup>, and the silylation conditions were 105 °C, 1.5 min, 10 Torr. The model assumed diffraction-limited optics, whereas the experimental image quality was limited by aberrations. The differences in aerial image may account for the differences in profile. For the experimental exposure, the fluence per pulse was calibrated at approximately 0.25 mJ/cm<sup>2</sup> per pulse.

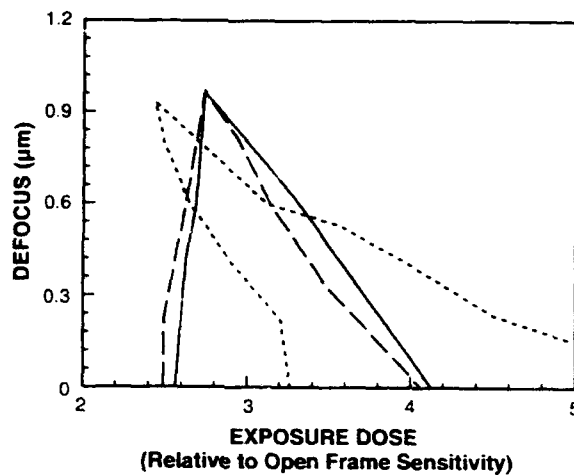


Figure 5. Exposure-defocus (E-D) trees for 0.25- $\mu\text{m}$  line-and-space patterns using 193-nm radiation,  $\text{NA}=0.5$ , and  $\sigma=0.6$ . The three curves correspond to the aerial image (smooth line), the silylation resist final profile (dotted line), and the bilayer resist (dashed line). Any exposure-defocus combination falling under the curve indicates a feature printed to within 10% of critical dimension.

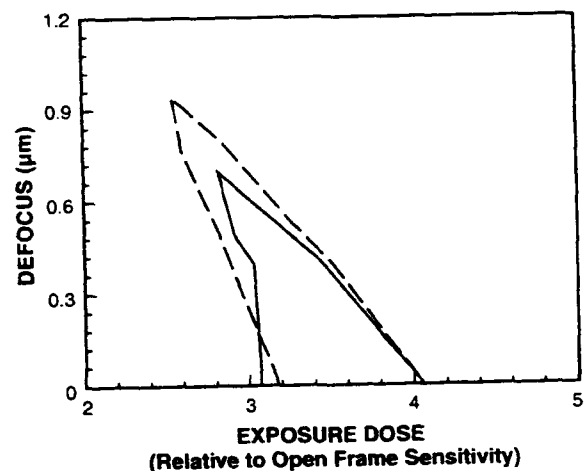
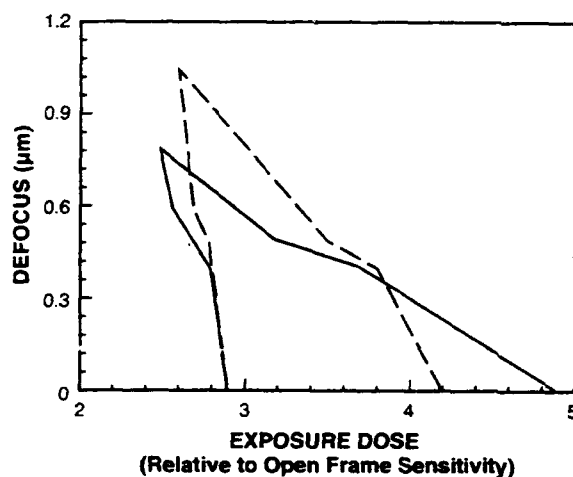
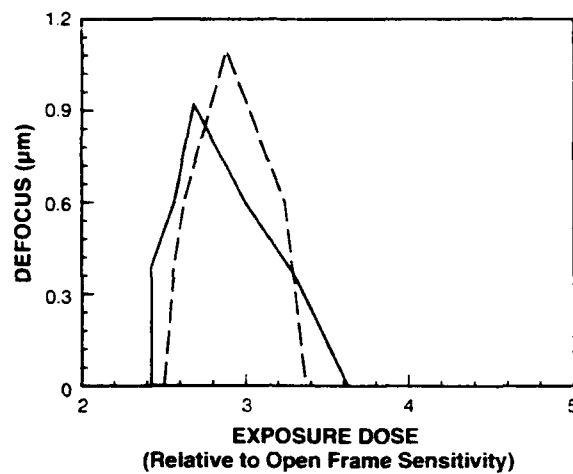
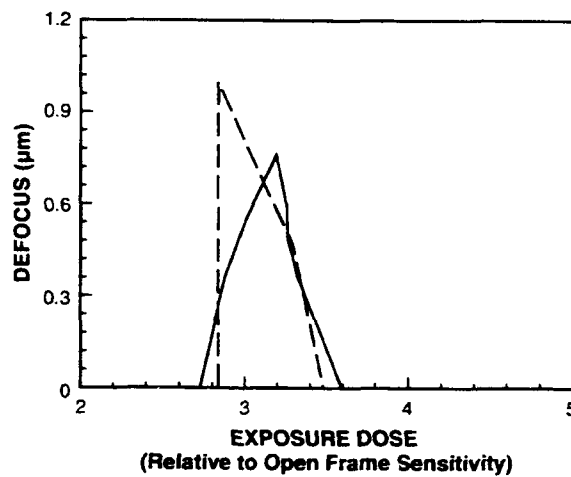


Figure 6. (a) E-D tree for 0.25- $\mu\text{m}$  line-and-space pattern printed in the silylation resist using 193 nm and 0.5 NA. The solid line is for circular illumination ( $\sigma \approx 0.6$ ) whereas the dashed line is for annular illumination ( $\sigma_i = 0.4$  and  $\sigma_o = 0.6$ ). (b) E-D tree for 0.18- $\mu\text{m}$  line-and-space pattern printed as in (a).



(a)



(b)

Figure 7. (a) E-D tree for 0.25- $\mu\text{m}$  line-and-space pattern printed in the bilayer resist using 193-nm radiation and 0.5 NA. The solid line is for circular illumination ( $\sigma = 0.6$ ) whereas the dashed line is for annular illumination ( $\sigma_i = 0.4$  and  $\sigma_o = 0.6$ ). (b) E-D tree for 0.18- $\mu\text{m}$  line-and-space pattern printed as in (a).